All-silicon photonic crystal photoconductor on silicon-on-insulator at telecom wavelength

Laurent-Daniel Haret,[1,*] Xavier Checoury,[1] Zheng Han,[1] Philippe Boucaud,[1] Sylvain Combrié,[2] and Alfredo De Rossi[2]

[1] *Institut d'Electronique Fondamentale, Bâtiment 220, Univ. Paris Sud, CNRS, UMR 8622, F-91405 Orsay, France*
[2] *Thales Research and Technology, 1 avenue Augustin Fresnel, 91767 Palaiseau, France*
**laurent.haret@ief.u-psud.fr*

Abstract: We demonstrate an all-silicon photodetector working at telecom wavelength. The device is a simple metal-semiconductor-metal detector fabricated on silicon-on-insulator. A two-dimensional photonic crystal nanocavity (Q = 60,000) is used to increase the response that arises from the linear and two-photon absorption of silicon. The responsivity of the detector is about 20 mA/W and its bandwidth is larger than 1 GHz.

©2010 Optical Society of America

OCIS codes: (230.5298) Photonic crystals; (230.5160) Photodetectors.

References and links

1. M. T. Hill, H. J. S. Dorren, T. De Vries, X. J. M. Leijtens, J. H. Den Besten, B. Smalbrugge, Y.-S. Oei, H. Binsma, G.-D. Khoe, and M. K. Smit, "A fast low-power optical memory based on coupled micro-ring lasers," Nature **432**(7014), 206–209 (2004).
2. M. El kurdi, P. Boucaud, S. Sauvage, G. Fishman, O. Kermarrec, Y. Campidelli, D. Bensahel, G. Saint-Girons, I. Sagnes, and G. Patriarche, "Silicon-on-insulator waveguide photodetector with Ge/Si self-assembled islands," J. Appl. Phys. **92**(4), 1858 (2002).
3. M. Oehme, J. Werner, M. Jutzi, G. Wöhl, E. Kasper, and M. Berroth, "High-speed germanium photodiodes monolithically integrated on silicon with MBE," Thin Solid Films **508**(1-2), 393–395 (2006).
4. D. Ahn, C. Y. Hong, J. Liu, W. Giziewicz, M. Beals, L. C. Kimerling, J. Michel, J. Chen, and F. X. Kärtner, "High performance, waveguide integrated Ge photodetectors," Opt. Express **15**(7), 3916–3921 (2007).
5. L. Vivien, M. Rouvière, J. M. Fédéli, D. Marris-Morini, J. F. Damlencourt, J. Mangeney, P. Crozat, L. El Melhaoui, E. Cassan, X. Le Roux, D. Pascal, and S. Laval, "High speed and high responsivity germanium photodetector integrated in a Silicon-On-Insulator microwaveguide," Opt. Express **15**(15), 9843–9848 (2007).
6. T. Yin, R. Cohen, M. M. Morse, G. Sarid, Y. Chetrit, D. Rubin, and M. J. Paniccia, "31 GHz Ge n-i-p waveguide photodetectors on Silicon-on-Insulator substrate," Opt. Express **15**(21), 13965–13971 (2007).
7. M. W. Geis, S. J. Spector, M. E. Grein, R. T. Schulein, J. U. Yoon, D. M. Lennon, S. Deneault, F. Gan, F. X. Kaertner, and T. M. Lyszczarz, "CMOS-Compatible all-Si high-speed waveguide photodiodes with high responsivity in near-infrared communication band," IEEE Photon. Technol. Lett. **19**(3), 152–154 (2007).
8. J. D. B. Bradley, P. E. Jessop, and A. P. Knights, "Silicon waveguide-integrated optical power monitor with enhanced sensitivity at 1550 nm," Appl. Phys. Lett. **86**(24), 241103 (2005).
9. Y. Liu, C. W. Cho, W. Y. Cheung, and H. K. Tsang, "In-line channel power monitor based on helium ion implantation in Silicon-on-insulator waveguides," IEEE Photon. Technol. Lett. **18**(17), 1882–1884 (2006).
10. J. K. Doylend, P. E. Jessop, and A. P. Knights, "Silicon photonic resonator-enhanced defect-mediated photodiode for sub-bandgap detection," Opt. Express **18**(14), 14671–14678 (2010).
11. T. K. Liang, H. K. Tsang, I. E. Day, J. Drake, A. P. Knights, and M. Asghari, "Silicon waveguide two-photon absorption detector at 1.5 µm wavelength for autocorrelation measurements," Appl. Phys. Lett. **81**(7), 1323 (2002).
12. J. Bravo-Abad, E. P. Ippen, and M. Soljačić, "Ultrafast photodetection in an all-silicon chip enabled by two-photon absorption," Appl. Phys. Lett. **94**(24), 241103 (2009).
13. Y. Akahane, T. Asano, B.-S. Song, and S. Noda, "High-Q photonic nanocavity in a two-dimensional photonic crystal," Nature **425**(6961), 944–947 (2003).
14. E. Kuramochi, H. Taniyama, T. Tanabe, A. Shinya, and M. Notomi, "Ultrahigh-**Q** two-dimensional photonic crystal slab nanocavities in very thin barriers," Appl. Phys. Lett. **93**(11), 111112 (2008).
15. Z. Han, X. Checoury, D. Néel, S. David, M. El Kurdi, and P. Boucaud, "Optimized design for 2×10^6 ultra-high Q siliconphotonic crystal cavities," Opt. Commun. **283**(21), 4387–4391 (2010).
16. T. Tanabe, H. Sumikura, H. Taniyama, A. Shinya, and M. Notomi, "All-silicon sub-Gb/s telecom detector with low dark current and high quantum efficiency on chip," Appl. Phys. Lett. **96**(10), 101103 (2010).
17. A. R. Zain, N. P. Johnson, M. Sorel, and R. M. De La Rue, "Ultra high quality factor one dimensional photonic crystal/photonic wire micro-cavities in silicon-on-insulator (SOI)," Opt. Express **16**(16), 12084–12089 (2008).

#134167 - $15.00 USD Received 30 Aug 2010; revised 22 Oct 2010; accepted 26 Oct 2010; published 1 Nov 2010

18. E. Kuramochi, H. Taniyama, T. Tanabe, K. Kawasaki, Y.-G. Roh, and M. Notomi, "Ultrahigh-Q one-dimensional photonic crystal nanocavities with modulated mode-gap barriers on SiO_2 claddings and on air claddings," Opt. Express **18**(15), 15859–15869 (2010).
19. Y. Tanaka, T. Asano, R. Hatsuta, and S. Noda, "Investigation of point-defect cavity formed in two-dimensional photonic crystal slab with one-sided dielectric cladding," Appl. Phys. Lett. **88**(1), 011112 (2006).
20. E. Kuramochi, M. Notomi, S. Mitsugi, A. Shinya, T. Tanabe, and T. Watanabe, "Ultrahigh-**Q** photonic crystal nanocavities realized by the local width modulation of a line defect," Appl. Phys. Lett. **88**(4), 041112 (2006).
21. A. F. Oskooi, D. Roundy, M. Ibanescu, P. Bermel, J. D. Joannopoulos, and S. G. Johnson, "Meep: A flexible free-software package for electromagnetic simulations by the FDTD method," Comput. Phys. Commun. **181**(3), 687–702 (2010).
22. X. Checoury, S. Enoch, C. Lopez, and A. Blanco, "Stacking patterns in self-assembly opal photonic crystals," Appl. Phys. Lett. **90**(16), 161131 (2007).
23. M. Dinu, F. Quochi, and H. Garcia, "Third-order nonlinearities in silicon telecom wavelengths," Appl. Phys. Lett. **82**(18), 2954–2956 (2003).
24. P. Barclay, K. Srinivasan, and O. Painter, "Nonlinear response of silicon photonic crystal microresonators excited via an integrated waveguide and fiber taper," Opt. Express **13**(3), 801–820 (2005).
25. N. Matsuda, R. Shimizu, Y. Mitsumori, H. Kosaka, A. Sato, H. Yokoyama, K. Yamada, T. Watanabe, T. Tsuchizawa, H. Fukuda, S. Itabashi, and K. Edamatsu, "All-optical phase modulations in a silicon wire waveguide at ultralow light levels," Appl. Phys. Lett. **95**(17), 171110 (2009).

1. Introduction

The great interest in all-optical interconnects is triggered by the idea that it should lead to the conception of small, low-cost devices that will convey and process numerical data at very low working power [1]. The on-chip integration of these technologies with electrical micro-circuits will reduce the energy cost of optical to electrical signal conversion. As silicon is the major material used for electronic circuits, silicon photonics has become a very active research field, even though it is challenging to use silicon as an active material in the telecommunication window. Silicon-on-insulator (SOI) is indeed a very interesting platform for photonics but Si has an indirect electronic band gap, and is transparent at telecom wavelengths (λ = 1550 nm). Photodetection on chip in the telecom band thus requires the monolithic integration of a material like silicon-germanium self-assembled islands [2], or pure germanium. High responsivities around 1 A/W and high speed operation above 40 GHz have been recently demonstrated using CMOS integrated waveguides with germanium as the absorbing material [3–6].

An all-silicon approach however represents a major breakthrough because of its simplicity. Devices based on the linear absorption related to the introduction of defects states in implanted silicon have been employed to demonstrate high-responsivity *p-i-n* photodiodes [7–9]. The latter method can also be used in conjunction with a resonator to improve performances [10]. Here we explore another resonant approach where silicon is not implanted and where the absorption mechanism is not limited to linear absorption. This can be achieved since, at high optical densities, two-photon absorption (TPA) becomes significant in silicon. Silicon waveguide two-photon absorption detectors at 1.5 µm have been proposed [11,12]. Presently, the best way to reach high optical densities at a reasonable working power is to use photonic crystal (PhC) cavities that have a very high quality factor and a small mode volume. The experimental quality factors (Q) of these can be higher than 2 million with a mode volume still comparable to $(\lambda/n)^3$ [13–15]. In these conditions, linear absorption and TPA are enhanced and become detectable for an input power lower than 1 µW [16]. This remarkable effect has been used to create a photodetector built in a suspended structure with a *p-i-n* junction [16]. Moreover, it can lead to very compact resonant devices as opposed to standard waveguide approaches or even ring resonators. Though the photonic crystal approach is still not comparable to the implanted silicon approach in terms of responsivity or overall efficiency, it is very compact, which makes it favorable for on-chip integration and promising for reaching very-high speed operation. Also, because silicon is not implanted, it is possible to keep a high optical quality factor and to achieve highly wavelength-selective detection. Morevover, the main feature here is the non-linearity provided by TPA that may lead to applications such as noise reduction and numerical signal processing.

#134167 - $15.00 USD Received 30 Aug 2010; revised 22 Oct 2010; accepted 26 Oct 2010; published 1 Nov 2010
(C) 2010 OSA

In this article, we show that a simple SOI photonic crystal structure with a metal-semiconductor-metal (MSM) junction can also achieve photodetection in the telecom band. This all-silicon photodetector entirely resting on silica exhibits a responsivity of 17 mA/W and a frequency cutoff larger than 1 GHz.

2. Design and fabrication

The larger quality factors in PhC cavities are reached for 2D suspended air/Si/air structures while in the SOI case, the highest experimental quality factors ever demonstrated are about 360,000 [17,18]. This is because of the low index contrast between Si and SiO_2, and also because there is no complete photonic band gap in structures on oxide [19]. However, for a detector operating at a speed exceeding 10 GHz, it is necessary to have a cavity lifetime $\lambda Q / 2\pi c$ smaller than 100 ps, which yields $Q < 10^5$, a value that is ten times lower than the Q of suspended structures. Taking this into account, the use of a SOI structure becomes particularly advantageous in terms of fabrication simplicity, thermal management and future integration in fabrication processes at industry level. Our design for the cavity is as in [20]: a triangular lattice of air holes in silicon rests on a silica layer. A W0.98 waveguide (the barrier waveguide) is built into the structure by omitting a row of holes in the ΓK direction. At the center, the width of the waveguide is modulated smoothly which makes a cavity that resonates at a frequency c/λ smaller than the cutoff frequency of the barrier waveguide. Light is coupled into the sample by a 780 nm wide Si on SiO_2 waveguide and the cavity is loaded by evanescent coupling through the barrier waveguide as shown in Fig. 1 (a).

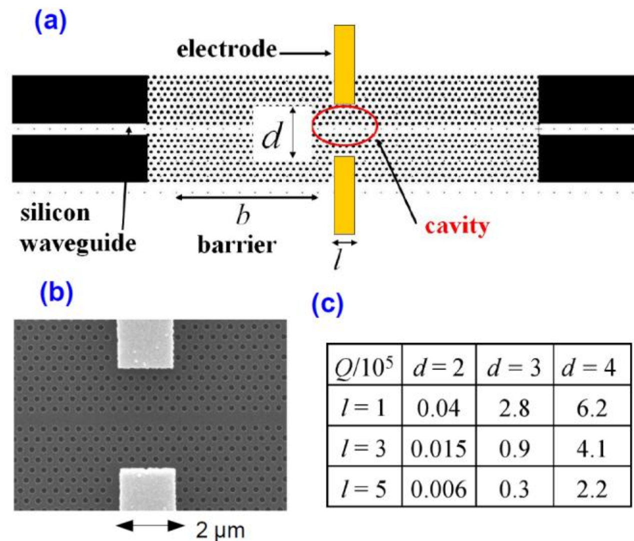

$Q/10^5$	$d = 2$	$d = 3$	$d = 4$
$l = 1$	0.04	2.8	6.2
$l = 3$	0.015	0.9	4.1
$l = 5$	0.006	0.3	2.2

Fig. 1. (a) Schematic description of the detector (b) SEM view of the cavity and electrodes (c) Simulated Q for different electrode geometries in the suspended cavity case, in units of 100 000.

Detection of free carriers generated by absorption is performed by applying a continuous bias on metallic contacts near the cavity. We designed these contacts as two rectangular gold electrodes (Fig. 1 (b)). The detector is a metal-semiconductor-metal structure that should behave as a photoconductor. Another possibility is to apply an electric field through a lateral *p-i-n* junction [16]. The MSM structure is easier to fabricate and may have some advantages in terms of carrier collection speed because there is no speed limitation due to transport by diffusion, as in the *p-i-n* case.

Putting a metallic conductor near the cavity might dramatically reduce its quality factor and make the detection principle totally inefficient. In order to evaluate the impact of gold on the optical performances of the cavity, we have performed a three-dimensional finite

#134167 - $15.00 USD Received 30 Aug 2010; revised 22 Oct 2010; accepted 26 Oct 2010; published 1 Nov 2010
(C) 2010 OSA

difference time domain (3D-FDTD) simulation of the optical properties in the case of a SOI structure, and in the case of a suspended structure. The Meep software [21] calculated the electrical field of the resonant modes from which the Q was deduced with a home-made numerical method [22]. The model for metal was a complex dielectric constant. The geometry of the electrodes is described by two parameters l and d, l being the width of the electrode expressed in units of PhC period a, and d being the distance between the electrode and the cavity center, expressed as a number of rows that is to say in units of $\sqrt{3}a/2$. In the suspended structure case, the simulation shows that the quality factor strongly depends on the electrode geometry: the intrinsic simulated Q is 42×10^6 while metallized cavity Q is greater than 10^5 only if $d > 3$ (see Table on Fig. 1 (c)). In the SOI case, when $d > 3$, the metallized cavity Q is limited only by the simulated intrinsic $Q = 10^5$, thanks to the small spatial extension of the cavity mode. Therefore, we fabricated a structure for $d = 4$ and $l = 4$.

Far from the cavity, the electrodes are enlarged into a 100×100 µm square for current collection. The fabrication parameters are as following: crystal lattice $a = 420$ nm, hole radius $r = 104$ nm, thickness of silicon layer $h = 200$ nm. Fabrication needs only two steps: we first make the PhC and the silicon waveguide with a first electron beam lithography followed by dry etching [15]. Then we fabricate the electrodes: the metal contact zone is patterned by a second lithography, a 10 nm thick layer of titanium that sticks on silicon and a 180 nm thick layer of gold are evaporated on the sample. A lift-off technique finally removes the metal, except in the zones that were insulated. The main difficulty is to align the second lithography with the PhC structures on the sample (Fig. 1 (b))

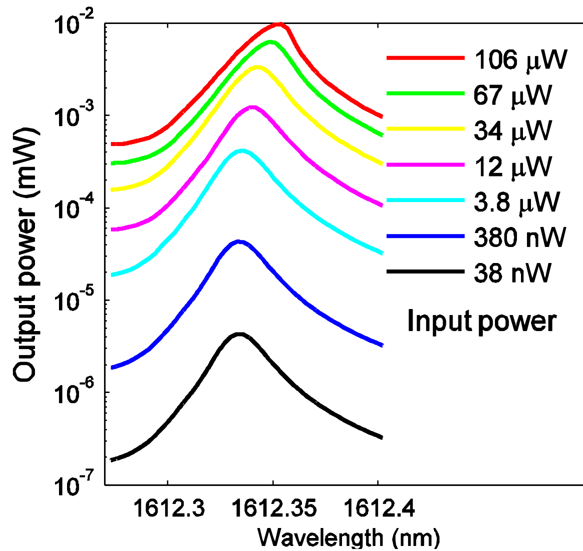

Fig. 2. Transmission spectra of the cavity at different input powers (Q = 58,000).

3. Demonstration of detection in continuous regime

The photodetectors were probed by a tunable continuous mode laser source. A power meter collects the output, thus measuring the spectral transmission of the cavities (Fig. 2). The coupling losses due to the experimental set-up are first measured at wavelengths beneath the barrier cutoff. These losses are typically 25 dB and from now on, they will be taken into account as an offset in order to consider the significant quantities only, i.e., the input power, defined as the optical power in the PhC waveguide immediately after the ridge waveguide (see Fig. 1 (a)) and the output power defined as the power in the PhC waveguide before the exit ridge waveguide. The cutoff wavelength is around 1605 nm and the cavity resonant wavelength about 1610 nm. We measured several samples which had different barrier

#134167 - $15.00 USD Received 30 Aug 2010; revised 22 Oct 2010; accepted 26 Oct 2010; published 1 Nov 2010
(C) 2010 OSA

waveguide lengths ($b = 8a$, $11a$, $14a$) and found the quality factors were $Q = 43\,000$, 58 000, 80 000 and the cavity transmission values were T_0 = 15%, 11%, 0.3% respectively. This shows experimentally that the quality factor is controlled by the barrier length, and confirms that it is not limited by the electrodes. The Q values are very high for a 2D PhC cavity built in SOI [17,19]. We will now concentrate on the intermediate sample (Q = 58,000). At a high input power, the transmission decreases and the spectra become asymmetrical, evidencing the generation of free carriers in the material (Fig. 2).

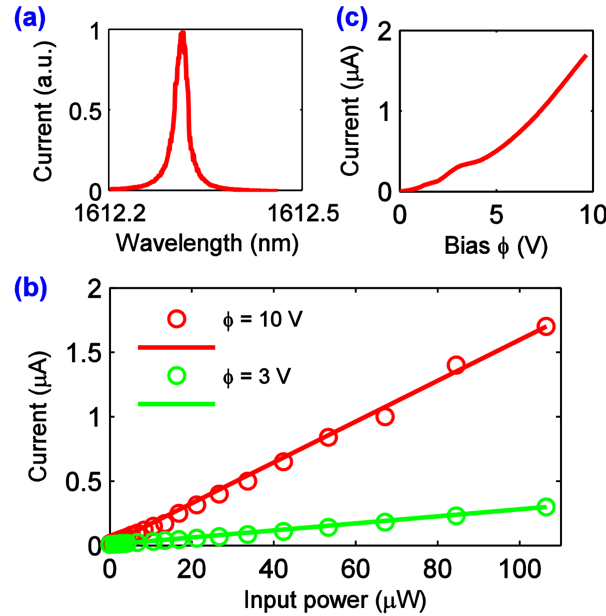

Fig. 3. (a) Photocurrent dependence vs. wavelength. Optical input power is 70 μW and bias is 10V (b) Photocurrent at optical resonance as a function of input power at 10 V and 3 V biases. (c) Resonant photocurrent depending on the bias at a 100 μW input power.

Metal tips are brought onto the gold square so that a continuous voltage can be applied, allowing us to measure an electrical current that depends on the optical input power, the wavelength and the bias. The current spectrum shows a resonant enhancement at the cavity wavelength (Fig. 3 (a)). It is possible to apply a 10 V bias to the sample without any damage. In the investigated conditions, i.e. for an input power lower than 100 μW, linear absorption is dominant and the dependence of the resonant photocurrent on the input power (Fig. 3 (b)) shows that the non-linear detector measured at 100 μW input power is equivalent to a linear detector with a responsivity of 4 mA/W at a 3 V bias and 17 mA/W at a 10 V bias. These values are reached whereas only a small part of the pump is effectively absorbed in the cavity. The current also increases with the bias: the device behaves as a photoconductor (Fig. 3 (b) and 3 (c)). Dark current is 12 nA under 10 V. With our set-up, we were able to measure a photocurrent corresponding to a fraction of nA at an input power as low as 10 nW. This means that with an integrated device processing the data and subtracting the dark current, the detector should work at very low input power in the continuous regime.

As our device was meant to be non-linear, we have to study more in detail how the photocurrent depends on the optical input. The current comes from two physical mechanisms: enhancement of linear absorption, and TPA. In the following equations, $n = 3.45$, q, P_{in}, P_{out}, T_0, U, $\beta = 8\times10^{-12}\,\text{mW}^{-1}$ [23] and α stand for silicon refraction index, elementary charge, input power, output power, transmission at low input, optical energy in the cavity, TPA coefficient and linear absorption coefficient. V_{TPA} is the volume associated with two-photon absorption [24] and it was calculated from the FDTD mode profile:

#134167 - $15.00 USD Received 30 Aug 2010; revised 22 Oct 2010; accepted 26 Oct 2010; published 1 Nov 2010
(C) 2010 OSA

$$V_{\text{TPA}} = \frac{\left(\int n^2 E^2 dr\right)^2}{\int_{\text{Si}} n^4 E^4 dr} = 0.67\ (\mu\text{m})^3. \quad (1)$$

Then the photocurrent is expressed as a polynomial function of the cavity energy U:

$$I_{\text{ph}} = \frac{qg}{\hbar\omega_0}\left[\alpha \frac{c}{n} U + \frac{\beta}{2}\left(\frac{c}{n}\right)^2 \frac{U^2}{V_{\text{TPA}}}\right]. \quad (2)$$

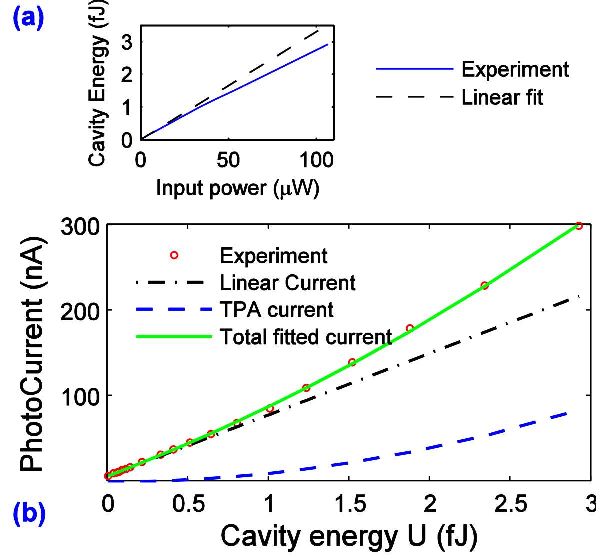

Fig. 4. (a) Cavity energy vs. optical input power. The dependence is sub-linear: the black dashed line shows the tangent at the origin (b) Photocurrent as a function of cavity energy, at a 3 V bias. The circles are the experimental values. The dashed line is the fitted TPA current, the dotted-dashed line is the linear current and the solid line is the total fitted current.

The gain g is here a number representing the ratio of the quantity of collected carriers per second (I_{ph} / q) to the generated carriers per second. It increases with the bias and depends on the diffusion properties of carriers out of the cavity.

We need to fit this model to the experimental data, therefore to evaluate U in some way. Because of the two-photon absorption and free carrier absorption effect, the theoretical dependence of U on the input power is not simply linear: as the power increases, the effective quality factor is reduced because of non-linear losses. One way of solving this difficulty is to consider the output power given directly by the experiment, as it depends linearly on the cavity energy through the lateral coupling coefficient:

$$U = \frac{2P_{\text{out}}Q}{\sqrt{T_0}\,\omega_0}. \quad (3)$$

With this method we can obtain the dependence of U on the input power, which is sub-linear as expected (Fig. 4 (a)). Then experimental data is fitted to Equ. (2), with only fitting parameters α and g. (Fig. 4 (b)). At a 3 V bias, linear absorption is found as $\alpha = 0.16$ dB/cm, which is the same order of magnitude than the value given in references [16,25]. This value does not change considerably when we perform the fit at another bias. g is 0.16 at 3V bias and could also be considered as the ratio of the carrier lifetime to the carrier collection time. If we roughly estimate the carrier lifetime in the cavity as 100 ps, the collection time would be around 625 ps. This value is much larger than the transit time between the electrodes $d^2 / \mu V$ where μ stands for electron mobility, as in a standard photoconductor: If we consider the

#134167 - $15.00 USD Received 30 Aug 2010; revised 22 Oct 2010; accepted 26 Oct 2010; published 1 Nov 2010
(C) 2010 OSA

standard electron mobility in silicon (0.145 $m^2V^{-1}s^{-1}$), the transit time at a 3 V applied bias is 30 ps. This means that our collection efficiency is not limited by the transit time but probably by the electric contacts. At this stage, a measurement of the carrier mobility in the PhC structure and the collection efficiency of the contacts need to be accurately evaluated before giving a rigorous evaluation of the carrier lifetime. A detailed study is in progress to determine the electrical characteristics of the metal-semiconductor junction in presence of a photonic crystal when direct and reverse bias are applied.

It is interesting to know what is the ratio between the linear photocurrent and the TPA photocurrent. The fit shows that in this particular case, contribution of TPA current in the overall current is about 30% at a 3 V bias. In order to theoretically increase the contribution of TPA, one could increase Q and reduce the TPA volume: Eq. (2) and (3) show that the ratio $I_{\mathrm{TPA}} / I_{\mathrm{linear}}$ scales with Q / V_{TPA}. From the modeling, we anticipate that the response should be 0.1 A/W for a 10 mW input power where two-photon absorption becomes dominant. This means that by tuning the optical parameters of the device, we should be able to get either a linear detector, or a much more quadratic one. In the former case, it will be suited for detection of analogical signals, while in the latter case, it could perform some noise reduction and pulse reshaping for digital communications.

4. Demonstration in variable regime

In order to get an estimate of the bandwidth of the device, we injected an input power signal $P_{in} = P_0(1+0.2\cos(2\pi ft))$ where frequency f ranges from 10 to 2000 MHz. We used a Mach-Zender interferometer to modulate the incident optical power. The current is amplified and analyzed in the temporal domain by an oscilloscope. Figure 5 (a) shows a screen shot of the modulation and photocurrent signal for f = 600 MHz. One can observe a small non linearity on the photocurrent signal due to the quadratic TPA term in the response. We also used a network analyzer that could sweep over the values of f and measure the intensity of the photocurrent at the same time. The intensity of the optical input as a function of f was also measured by the network analyzer via a photodiode. The normalized dependence of the response as a function of the excitation frequency is shown in Fig. 5 (b). The bandwidth is the frequency at which the signal becomes two times smaller than its peak value. We find a cutoff frequency of 1.1 GHz, which is about one order of magnitude larger than the 0.1 Gbit/s operation demonstrated for a *p-i-n* photonic crystal detector [16], though we are aware that in the latter case, the result was obtained for an input light alternating between full extinction and full illumination. This value is still smaller than the optical bandwidth $\omega_0 / Q = 20$ GHz. However, the experimental conditions for this measurement were not ideal, as the detector was not matched to the external electric circuit 50 Ω impedance and the design and fabrication process of electric contacts were not optimized for current collection. For all these reasons, we expect to significantly improve the cutoff frequency and operation speed of the MSM photonic crystal detector in the future.

#134167 - $15.00 USD Received 30 Aug 2010; revised 22 Oct 2010; accepted 26 Oct 2010; published 1 Nov 2010
(C) 2010 OSA

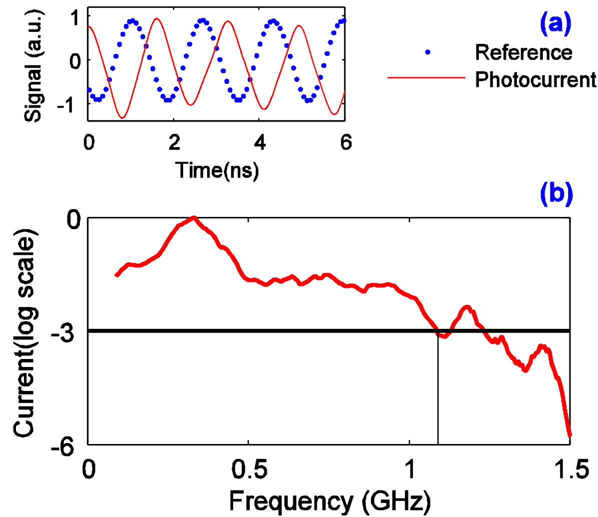

Fig. 5. (a) Input signal (dotted line) and detector signal (solid line) for f = 600 MHz. The applied bias is 7 V and the input power is 30 µW (b) Normalized response of the detector vs. modulation frequency. The −3 dB cutoff occurs at 1.1 GHz (7 V bias and 30 µW input power).

5. Conclusion

We have demonstrated an all-silicon wavelength-selective photoconductor fabricated on silicon-on-insulator with a MSM junction. The detector footprint is very small (15×10 µm if we consider the photonic crystal area). A responsivity as large as 17 mA/W has been achieved around 1.6 µm due to strong optical confinement, and it can operate for a continuous wave input power lower than 10 nW. In variable regime, it can operate above 1 GHz. The collection time is not limited by a region where carrier transport is diffusive as in the *p-i-n* junction; therefore we hope to significantly improve the bandwidth by optimizing the electrical contacts. The selectivity in wavelength could lead to the conception of a compact on-chip spectrometer over the telecom C-band. This demonstration on a silicon-on-insulator platform opens promising perspectives for resonant all-silicon integrated detectors operating in the telecommunication band with a high bandwidth, since a non-linear process such as two-photon absorption may allow to perform some basic signal processing tasks such as noise reduction and pulse reshaping.

Acknowledgments

This work was supported by RTRA Triangle de la Physique through the DESIRABLE project. S. Combrié and A. de Rossi acknowledge the EC project COPERNICUS (FP-ICP-249012).

#134167 - $15.00 USD Received 30 Aug 2010; revised 22 Oct 2010; accepted 26 Oct 2010; published 1 Nov 2010
(C) 2010 OSA